Domain-Specific Effector Interactions within the Central Cavity of Human Adult Hemoglobin in Solution and in Porous Sol−Gel Matrices: Evidence for Long-Range Communication Pathways[†,‡]

Eric S. Peterson,[§,||] Roman Shinder,[§] Imran Khan,[§] Laura Juczszak,[§] Jiaqian Wang,[§] Belur Manjula,[§] Seetharama A. Acharya,[§] Celia Bonaventura,[⊥] and Joel M. Friedman*[,§]

Department of Physiology and Biophysics, Albert Einstein College of Medicine, Bronx, New York 10461, and Duke University Marine Laboratory, Nicolas School of the Environment and Earth Sciences, 135 Duke Marine Lab Road, Beaufort, North Carolina 28516-9721

Received August 19, 2003; Revised Manuscript Received February 26, 2004

ABSTRACT: The water-filled central cavity of human adult hemoglobin (Hb A) is the binding or interaction site for many different allosteric effectors. Oxygen binding titrations reveal that pyrenetetrasulfonate (PyTS), a fluorescent analogue of 2,3-diphosphoglycerate, behaves like an allosteric effector. The ligation state, pH, and concentrations of other effectors (IHP, L35, and chloride) alter PyTS fluorescence for both solution-phase and sol−gel-encapsulated Hb samples. These conditions also alter the resonance Raman spectra and rates of geminate recombination of CO-ligated Hb. Together, these results demonstrate that there are conformational and functional consequences resulting from interactions between specific domains of the central cavity and individual effectors as well as from long-range synergistic effects that are mediated through the central cavity.

The reactivity of many proteins is subject to modulation through the binding of small ions or molecules termed effectors. The most dramatic examples of this class of phenomena include allosteric effectors that alter the equilibrium distribution of functionally distinct quaternary structures. The allosteric modulation by inorganic phosphates, protons, and anions of the binding of a ligand to hemoglobin (Hb) is one of the best-studied examples of this general phenomenon. A significant component of this effect is readily explained by preferential binding of an effector to a given quaternary structure. This preferential binding induces a shift in population between high- and low-affinity quaternary states and has been the basis for explaining the most obvious functional changes induced in Hb upon effector binding. It has also been observed that the reactivity of Hb maintained within a given quaternary state is subject to modulation by the addition of effector molecules (*1*−*4*). The mechanism of how effectors alter ligand reactivity for the low-affinity T and high-affinity R quaternary states of hemoglobin is not fully understood. The issue of how effector binding modulates reactivity within a given quaternary state raises intriguing questions about the conformational and functional plasticity that exists within a given protein structure.

A full picture describing in detail the mechanism through which a given effector alters the reactivity of a protein within a given quaternary state must identify (i) where and how strongly the effector binds, (ii) the conformational and dynamical consequences of effector binding, and (iii) how these conformational and dynamical changes affect ligand reactivity. This study focuses on these questions with respect to how several different allosteric effectors interact with human adult hemoglobin (Hb A),[1] primarily in its fully ligated form.

The three effectors that have been studied are inositol hexaphosphate (IHP), L35 {2-[4-(3,5-dichlorophenylureido)-phenoxy]-2-methylpropionic acid} (*5*), and chloride (Cl^-). For deoxy Hb A, all three effectors operate through interactions with residues lining the water-filled central cavity of Hb A. IHP binds to the $\beta\beta$ end of the central cavity at the same site to which the physiologically important effector DPG (2,3-diphosphoglycerate) binds (*6*, *7*). This site is often termed either the DPG binding site or the β cleft of the central cavity. L35, a modified and more potent version of bezafibrate (*8*), has primary binding sites toward the α end of the central cavity as well as weaker binding sites toward the β end of the central cavity (*5*). Crystallographic evidence has been presented for inorganic anion binding sites at the

[†] This work was supported in part by National Institutes of Health Grants HL71064, GM58890, and EB00296 and by the W. M. Keck Foundation.

[‡] This work is dedicated to the memory of our friend and colleague, Dr. Eraldo Antonini, a pioneer in the study of hemoglobin structure−function relationships who died 20 years ago.

* To whom correspondence should be addressed: Department of Physiology and Biophysics, Albert Einstein College of Medicine, 1300 Morris Park Ave., Bronx, NY 10461. Phone: (718) 430-3591. Fax: (718) 430-8819. E-mail: jfriedma@aecom.yu.edu.

[§] Albert Einstein College of Medicine.

[||] Present address: Department of Chemistry, Bowdoin College, Brunswick, ME 04011-8466.

[⊥] Nicolas School of the Environment and Earth Sciences.

[1] Abbreviations: Hb A, human adult hemoglobin; PyTS, pyrenetetrasulfonate; DPG, 2,3-diphosphoglycerate; IHP, inositol hexaphosphate; CO, carbon monoxide; GR, geminate recombination; GY, geminate yield; L35, 2-[4-(3,5-dichlorophenylureido)phenoxy]-2-methylpropionic acid; bezafibrate, 2-{4-[2-(4-chlorobenzamido)ethyl]phenoxy}-2-methylpropanoic acid.

10.1021/bi035481o CCC: $27.50
Published on Web 04/02/2004

N-termini of the α subunits of human deoxyhemoglobin in addition to sites in the central cavity (*86*). However, except in instances where Hb A mutations produce especially favorable binding sites, Cl^- does not bind tightly enough to be visualized in X-ray crystal structures (*1*, *9*−*12*).

It is well established that these three effectors decrease the oxygen affinity of Hb at the midpoint of oxygen binding (P_{50}) and at 5% low saturation (P_5), where the protein is typically in its T-state quaternary conformation. The structure-specific effects are hard to discern from oxygen affinity measurements because the contributions of the different species that comprise the equilibrium population of Hb A under oxygen titration conditions cannot be separated. In contrast, the geminate recombination of CO to photodissociated CO-ligated Hb A in solution under ambient conditions occurs within a temporal window of a few hundred nanoseconds (*9*−*11*). As a result, the geminate recombination overwhelmingly reflects the properties of the initial population of CO-ligated Hb A. It has been shown that the fraction of photodissociated molecules undergoing geminate recombination, the geminate yield (GY), is highly responsive to Hb conformation (*12*−*16*). Using double-pulse techniques, iron−metal hybrids, and effector-loaded partially ligated forms, it has been inferred that the GY varies from ∼0.50 in the R state to close to zero in the T state. More recently, porous sol−gels were used to trap the CO-bound T state of Hb A and directly confirm this conclusion (*17*−*19*). Many of these studies also show that in the presence of allosteric effectors, the GY decreases for the ligated, R state, of Hb A. We build upon these results in this study, where the GY is used to monitor the functional consequences of added effectors with an emphasis on competitive and synergistic effects between different effectors.

The results of the functional studies are correlated with the conformational consequences of added effectors as reflected in frequency changes of ν(Fe−His), the iron−proximal histidine stretching mode, observed for the 8 ns photoproduct of CO-ligated Hb A. As with the GY, this frequency (which for the 8 ns photoproduct reflects the initial conformation of the unphotolyzed ligated Hb A population) is highly responsive to the Hb conformation (*13*, *20*−*27*). The highest observed frequency at ∼230 cm^{-1} occurs for the photoproduct of an effector-free sample of CO-ligated Hb A (pH 6.5−9.0), whereas the lowest frequency occurs for T-state deoxy Hb A at ∼215 cm^{-1}. Intermediate values are observed for the photoproducts of ligated T-state species trapped in porous sol−gel matrices (*28*) and for deoxy or effector-bound R-state species (*17*, *21*, *24*, *29*−*31*). Perturbations of both R- and T-state species result in intermediate values that correlate with ligand reactivity, especially as reflected in the GY of the species in question (*17*, *23*, *32*, *33*).

The binding of an effector to Hb A can be followed directly when the binding produces a clear-cut change in either an effector or Hb-specific spectroscopic marker or a measure of some aspect of reactivity. Binding that does not engender such changes is not easily monitored since the effectors are often optically silent. An approach to studying effector binding that has proven to be successful utilizes fluorescent analogues of DPG (*34*−*38*). Upon binding, these analogues exhibit a large decrease in their fluorescence intensity and lifetime due to excited-state quenching by the nearby heme groups. The initial studies utilized HPTS (8-hydroxy-1,3,6-pyrenetrisulfonate). The use of HPTS is complicated in some instances because of the pH dependence of its fluorescence spectrum. The use of pH insensitive PyTS (1,3,6,8-pyrenetetrasulfonate) eliminates this potential complication (*38*). The previous studies addressed the binding of these analogue effectors to Hb A as a function of different ligation and oxidation states. Competition experiments in which the analogues were displaced from Hb by stronger binding effectors such as IHP were also described.

This study describes a more complete set of effector competition experiments using PyTS. Whereas the GY and Raman measurements expose the impact of different added effectors upon the heme and heme environment, the PyTS studies probe the DPG binding site. The premise behind these PyTS experiments is that the fluorescence changes provide a direct window into status of the DPG binding site as a function of not only heme ligation state but also the addition of effectors such as L35 that interact with Hb A as sites distal to the DPG binding site. Changes in the fluorescence intensity of PyTS bound to deoxy and CO Hb A upon addition of IHP, L35, or Cl, either individually or in combination, are observed. These data are used to assess how either individual effectors or combinations of effectors influence binding at the DPG binding site. Both competitive and additive effects are observed, providing evidence for relatively long-range communication pathways within the central cavity.

The PyTS studies in solution are restricted to equilibrium species. Encapsulation of Hb's within porous sol−gel matrices followed by the addition or removal of ligand has been shown to be a viable mechanism for trapping intermediate species of Hb A (e.g., ligated T or deoxy R) for sufficiently long periods to enable functional and spectroscopic characterization (*18*, *19*, *28*, *39*−*42*). The study presented here also seeks to establish the feasibility of using PyTS as a probe of the DPG binding site in nonequilibrium states generated through encapsulation techniques. The results clearly demonstrate the compatibility of the two techniques, thus opening the door for future studies of binding of effectors to species likely to be functional intermediates.

MATERIALS AND METHODS

Materials. The fluorophore PyTS was purchased from Molecular Probes and used without further purification. The concentration of the probe in solution was determined using an extinction coefficient of 48.7 mM^{-1} cm^{-1} at 375 nm. Purified L35 was obtained as a generous gift from Dr. I. Lalezari.

HPLC-purified Hb A was prepared as previously described (*43*). Concentrated solutions of the protein were dialyzed against appropriate buffers to prepare samples at specific pH values. Also examined is the cross-linked derivative of Hb A prepared using bis(3,5-dibromosalicyl)fumarate in a reaction with deoxy Hb A. X-ray crystallographic studies (*44*) show that the fumaryl cross-link connects the Lys99 residues in $\alpha_1\alpha_2$ subunits, thus spanning the central cavity of the tetramer. Both of these lysines are located within a cluster of charged residues very near the middle of the Hb molecule. This site is also a significant part of the primary binding site for L35. This cross-linked Hb, designated ααXL Hb A

in this study, was prepared using the original published protocol (*44*).

CO-ligated Hb derivatives were prepared by gently passing chemically pure carbon monoxide gas over the surface of solutions of the starting oxy Hb samples. Deoxy Hb was prepared by first flushing an oxy Hb sample with pure nitrogen gas and then adding between 1 and 2 equiv of sodium dithionite. Complete conversion of the samples to either the deoxy or CO derivative was verified using the visible absorption spectrum, which was also used to establish Hb concentrations. Hb samples containing any of the effectors, including PyTS, were prepared by adding small aliquots of a concentrated stock solution of effector to the much larger volume of the Hb solution to generate samples that were 0.50 mM in heme with varying stoichiometric amounts of added effector. The experiments designed to test the effect of added nonfluorescent effectors on the binding of PyTS utilized a starting sample of Hb A with 1 equiv (based on the concentration of tetramer) of added PyTS.

Sol−gel-encapsulated Hbs (as either deoxy or CO derivatives) were prepared from tetramethoxylsilane (TMOS) using a previously described protocol in which a small amount of glycerol is added to the standard starting ingredients (*18*, *28*). The sol−gel samples were prepared as a thin (≤1 mm) layer on a single inner surface of a stoppered 10 mm quartz cuvette. The effector-free sol−gel samples, once appropriately aged, were immersed in buffer to which aliquots of a concentrated effector solution could be added to achieve the desired effector:tetramer concentration ratio within the gel. In all of the sol−gel measurements, a waiting period of up to several hours was used to ensure full equilibration. Although immediate changes in the fluorescence intensity indicated rapid diffusion of the added effectors (including PyTS) into the sol−gel matrix, in some instances the fluorescence continued to evolve over periods as long as a few hours due to the slow diffusion of the negatively charged effectors into the sol−gel matrix.

Oxygen Binding Measurements. Equilibrium oxygen binding curves for Hb A were determined tonometrically as described previously (*1*−*4*). For these studies, the HPLC-purified Hb was fully stripped of effectors and oxygen binding was then assessed in 0.05 M Bis-Tris in the presence and absence of added PyTS and/or DPT at several concentrations. Oxidized Fe^{3+} (met) Hb levels in these studies did not exceed 5%.

Geminate Recombination Measurements. Geminate recombination measurements were taken with an apparatus that uses the 8 ns second harmonic (532 nm) output pulses of a Nd:YAG laser running at 2 Hz to photodissociate the solution-phase COHb samples (0.8 mM in heme) contained in a 1 mm cuvette. The CO rebinding kinetics were monitored using the accompanying change in absorption of a 442 nm probe beam from a CW He:Cd laser that continuously interrogated the sample. The details of the apparatus, experimental conditions, and data analysis are found in previous publications (*17*, *18*, *28*).

Visible Resonance Raman Spectroscopy. The Soret band-enhanced resonance Raman spectrum of the 8 ns photoproduct of COHb in the presence and absence of allosteric effectors was produced using 8 ns pulses at 435 nm. These pulses are the first anti-Stokes shifted Raman lines generated by passing the 20 Hz second harmonic output of a Nd:YAG laser through a pressurized hydrogen cell. Details of the sample preparation, the apparatus, and the data processing are extensively described in earlier publications (*23*). Briefly, the samples for these experiments were approximately 1 mM in heme, poised at pH 6.5 using Bis-Tris acetate buffer, and saturated with CO before being loaded into a custom sample cell consisting of two windows mounted in a spinning holder cooled to ∼4 °C to avoid sample heating and photodegradation.

UV Resonance Raman Spectroscopy. The UV resonance Raman spectra of CO-saturated derivatives of Hb A and αα*XL Hb A as a function of added L35 were generated using a previously described apparatus (*45*). The Hb samples were all at a concentration of 0.5 mM heme in 50 mM Bis-Tris acetate buffer at pH 6.5. Data were collected on spinning and/or rastored samples contained within a 10 mm diameter quartz NMR tube chilled to 10 ± 4 °C to minimize photodamage. The excitation wavelength was 229 nm, and the incident laser power was 1.8 mW. Three 3 min acquisitions were gathered for each ligation state of each Hb variant over a frequency window of 820−1670 cm^{-1}. Absorption spectra were collected before and after exposure to the UV laser beam to confirm the absence of photodamage.

Fluorescence Measurements. The changes in the 355 nm excited fluorescence spectrum (scanned from 360 to 450 nm) of PyTS were monitored using a Shimadzu fluorimeter fitted with a front face excitation accessory. The commercially available front face accessory was further modified both to accommodate cuvettes and to yield reproducible intensity measurements. A front face excitation configuration was required to eliminate self-absorbance complications resulting from the high absorbance of the samples. The high absorbance of the samples was a consequence of the high Hb concentration required to minimize Hb dissociation into αβ dimers. Solution-phase measurements were taken on samples contained within 1 mm cuvettes, while the ∼1 mm thick sol−gel samples were contained on the inner face of a 10 mm cuvette. All measurements were repeated multiple times to ensure that the spectrum represented the fully equilibrated sample. Again, for the sol−gel samples, it often required tens of minutes, and occasionally hours, to reach a stable state.

RESULTS

Functional Studies of Geminate Recombination. Figure 1 shows the variation in the geminate recombination of CO Hb A at 25 °C and pH 6.5, with the addition of varied amounts of IHP to separate CO Hb A samples. As previously reported, IHP at a level of 5:1 (trace D) relative to effector-free Hb tetramers (trace A) reduces the geminate yield (fraction of heme sites undergoing geminate recombination, the rebinding of CO before it exits the protein) from a value of 27% in the native Hb to approximately 20% (a 26% reduction in the GY) (*13*, *17*, *46*, *47*); however, it can also be seen that with higher levels of IHP, the effect is lost (traces C and D). With IHP at 20:1 relative to Hb tetramers (trace B), there is almost no discernible effect of IHP on the geminate yield relative to the effector-free sample (trace A).

Figure 2 shows the geminate yield progressively decreases with increasing levels of L35. Additions of L35 above a ratio of 10:1 relative to Hb tetramers did not produce an

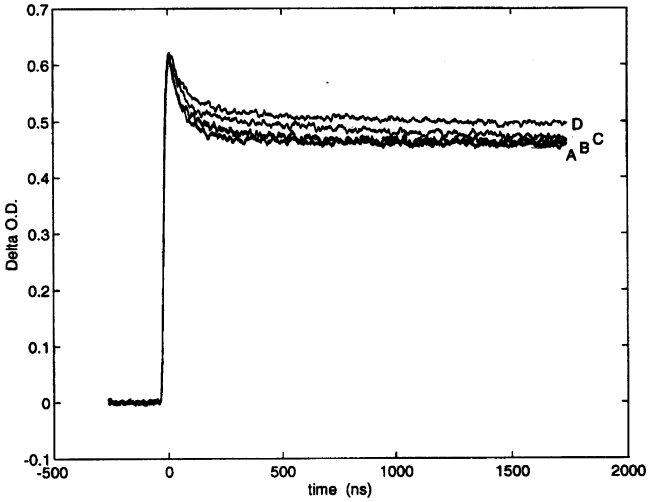

FIGURE 1: IHP dependence of the CO geminate recombination, expressed as a change in optical density with time, for CO Hb A. Sample conditions were 0.8 mM heme, Bis-Tris acetate buffer (50 mM, pH 6.5) at 25 °C. The trace labels correspond to the following IHP:Hb tetramer ratios: (A) 0:1, (B) 20:1, (C) 10:1, and (D) 5:1.

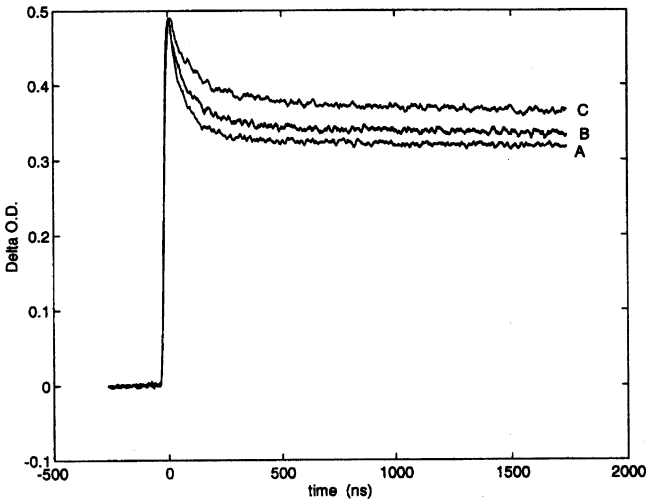

FIGURE 2: L35 dependence of the CO geminate recombination of CO Hb A. Conditions as in Figure 1. The trace labels correspond to the following L35:Hb tetramer ratios: (A) 0:1, (B) 5:1, and (C) 10:1.

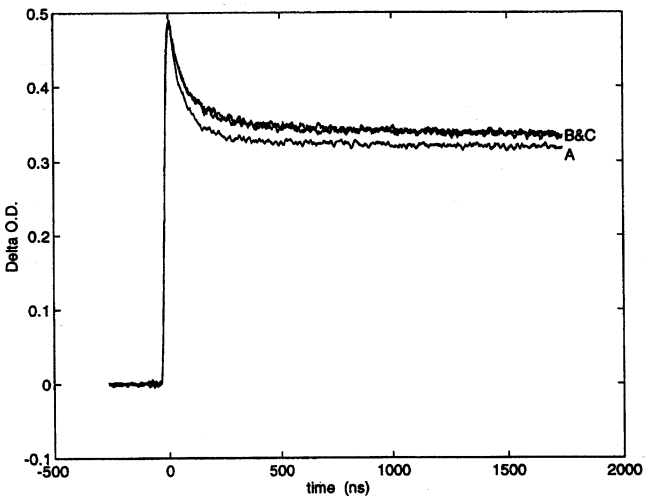

FIGURE 3: L35 vs Cl^- effects on the CO geminate recombination of CO Hb A. Conditions as in Figure 1. Effector:tetramer ratios were as follows: (A) 0:1, (B) L35 at 5:1, and (C) Cl^- at 1000:1.

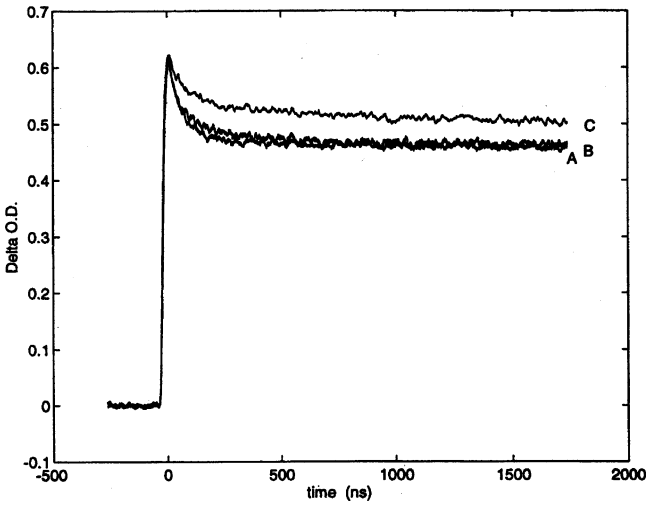

FIGURE 4: Combination effects of IHP and L35 on the CO geminate recombination of CO Hb A. Conditions as in Figure 1. The effector: Hb tetramer ratios are as follows: (A) 0:1, (B) IHP at 20:1, and (C) both IHP and L35 at 20:1.

experimentally significant change in the GY, so unlike the IHP case, there is no evidence of a reversal of the initial GY changes. Figure 3 displays data that indicate that the decrease in the geminate yield occurring with L35 at 5:1 can also be induced with Cl^- at 1000:1.

Figure 4 indicates that the addition of L35 to CO Hb A in the presence of IHP at 20:1 over the Hb tetramer concentration reverses the self-inhibitory effect of IHP (as seen in Figure 1) with respect to changes in the geminate yield. Regardless of whether the concentration of IHP is below or beyond the point where the reversal begins, the further addition of L35 reduces the geminate yield.

Conformational Effects Indicated by Resonance Raman Spectra. Figure 5 shows the 435 nm excited resonance Raman spectra of the 8 ns photoproduct of CO Hb A at pH 6.5 as a function of added allosteric effectors. The trends in the frequency of the iron−proximal histidine stretching mode, ν(Fe−His), parallel those seen in the geminate recombination measurements. The previously reported (*17*, *21*, *22*, *48*) effector-free value for ν(Fe−His) of 229 cm^{-1} is reduced to ∼226 cm^{-1} with the addition of IHP at both 5:1 and 10:1 effector:tetramer ratios (traces c and d). The presence of IHP at a 20:1 ratio relative to the Hb tetramer reverses the initial IHP effect (trace b), yielding a spectrum that is virtually identical to that of the effector-free sample (trace a). In contrast, the addition of L35 produces a decrease in the frequency of ν(Fe−His) with no reversal as its concentration is increased (traces e−g). The presence of L35 at 20:1 along with IHP at 20:1 (trace h) reverses the self-inhibitory effects of high levels of IHP. Last, the maximum frequency reduction, to a value of ∼221 cm^{-1}, is achieved with either L35 at ∼10:1 or a combination of both LC5 and IHP, similar to what was observed in the geminate data. Other effectors such as Cl^- at ∼1000:1 or PO_4^{2-} at ∼200:1 produce similar but smaller decreases in the frequency of ν(Fe−His) for the 8 ns photoproduct of CO Hb A at pH 6.5.

Conformational Alterations Indicated by UV Resonance Raman Measurements Showing L35 Interactions within the Central Cavity. The T-state binding site for L35 in deoxy Hb A has been well established using X-ray crystallography.

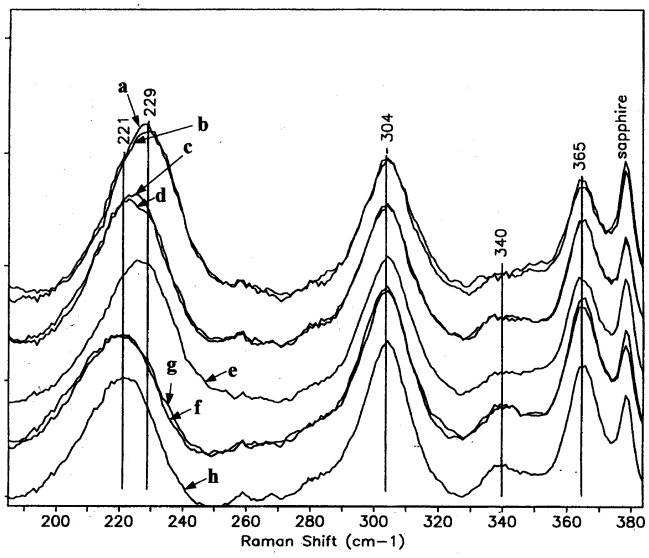

FIGURE 5: Excited resonance Raman spectrum (435 nm) of the 8 ns photoproduct of CO Hb A as a function of added allosteric effectors. Conditions as in Figure 1 except the temperature was maintained at approximately 4−10 °C and the Hb concentration was 1 mM in heme. The traces correspond to the following effector: Hb tetramer ratios: (a) 0:1, (b) IHP at 20:1, (c) IHP at 5:1, (d) IHP at 10:1, (e) L35 at 5:1, (f) L35 at 10:1, (g) L35 at 20:1, and (h) both L35 and IHP at 20:1. The line designated as sapphire is a reference signal originating from a sapphire window used as one of the two optical disks that sandwich the solution.

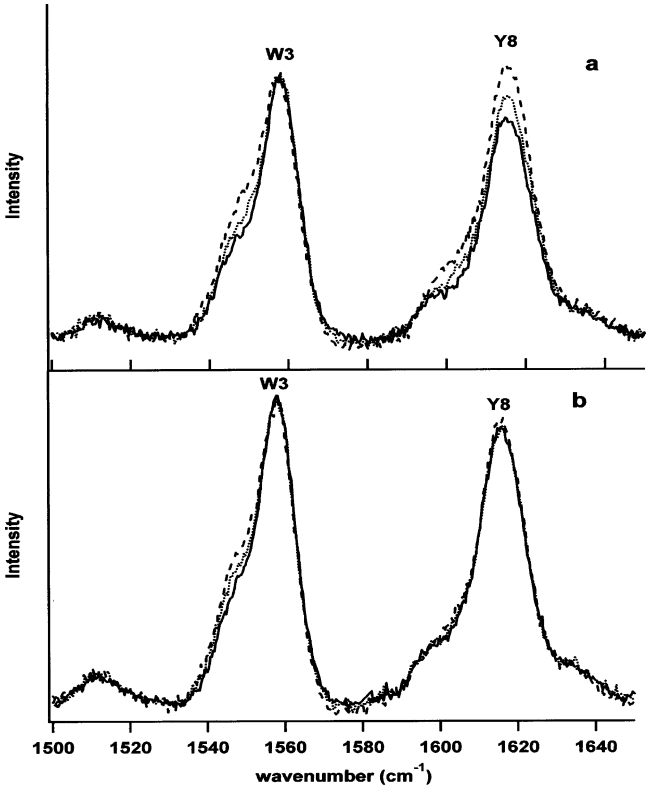

FIGURE 6: UV-excited (229 nm) resonance Raman spectrum of CO Hb A (a) and CO of ααXL Hb A (b) as a function of added L35 relative to tetramer concentration: (—) no added effectors, (• ••) L35 at 2:1, and (- - -) L35 at 4:1. Conditions as in Figure 1 but with the temperature maintained at approximately 4−10 °C.

It is less clear where and how L35 binds to the liganded R state of Hb A. The UV resonance Raman spectrum of Hb A contains features that are responsive to allosterically relevant perturbations within the central cavity and thus spectroscopic tools for evaluating the interactions of L35 with R-state solution-phase forms of CO Hb A. Figure 6 shows changes in the high-frequency region of the 229 nm excited UV resonance Raman (UVRR) spectrum of CO Hb A and the CO derivative of ααXL Hb A with the addition of L35. The intensity of the weak band at ∼1511 cm^{-1}, tentatively assigned to the 2xW18 mode (*49*), responds to quaternary structure change (deoxy T to ligated R) (*50*−*52*). Intensity changes in this mode appear to be reflective of changes involving Trp37β in the hinge region of the $\alpha_1\beta_2$ interface (*53*). The asymmetric band at ∼1560 cm^{-1} is the W3 band. The central component of this band is derived from Trp14α and Trp15β in the A helix (*50*, *51*, *54*, *55*). This component shows very little change in either intensity or frequency in going from deoxy T to ligated R. In contrast, the low-frequency shoulder at ∼1555 cm^{-1}, derived from Trp37β (*50*, *51*, *54*−*56*), shows a loss in intensity in going from deoxy T to ligated R. This intensity change is attributed to changes in the interaction between Trp37β and Asp94α. The tyrosine-associated Y8a band at ∼1620 cm^{-1} shifts to a lower frequency (∼2 cm^{-1}) in going from deoxy T to ligated R (*50*). This shift originates primarily from the R−T sensitive H bonding interaction between Tyr42α and Asp99β in the switch region of the $\alpha_1\beta_2$ interface (*54*, *57*, *58*). Intensity changes without frequency shifts in the Y8a band of modified Hb and R−T intermediates have been attributed to changes in the hydrogen bonding associated with penultimate tyrosines, Tyr140α and Tyr145β (*32*, *45*, *59*).

It can be seen in Figure 6 that the addition of L35 to CO Hb A (panel a) results in two changes in the spectrum. There is a clear L35-induced increase in the intensity of the Trp37β-associated low-frequency shoulder on the W3 band at ∼1555 cm^{-1}. This change is very similar to the change that occurs in this band in going from R to T. In this situation where L35 is added to CO Hb A, the other R → T signatures in the UV resonance Raman spectrum are absent. Neither the intensity of the 1511 cm^{-1} band nor the frequency of the Y8a band changes with the addition of L35. Instead, the only other change is an intensity increase in the tyrosine Y8a band with the addition of L35. It can be seen from the figure that for the cross-linked Hb, L35 still induces the changes in the shoulder of W3 (albeit a less pronounced change), but the intensity changes in Y8a are no longer apparent. As will be described in more detail below, this pattern of spectral changes is consistent with L35 interacting with residue side chains within the central cavity even in the liganded R-state population despite the volume limitations implied by crystallographic studies.

Influence of PyTS on the Binding of Oxygen to Hb. To evaluate the efficacy of PyTS as an effector, parallel oxygen binding studies were carried out at varied PyTS and DPG concentrations. As shown in Figure 7, the effect of PyTS is clearly like that of DPG in that it decreases the oxygen affinity at both pH 6.5 and 7.5, with greater changes at pH 7.5.

Some interesting differences in effector potency, revealed by the titrations shown in Figure 7, helped us define conditions that are appropriate for studies of competitive binding to this site. The objective is to be certain that the concentration conditions that are chosen correspond to having PyTS bound primarily at the DPG binding site and not at

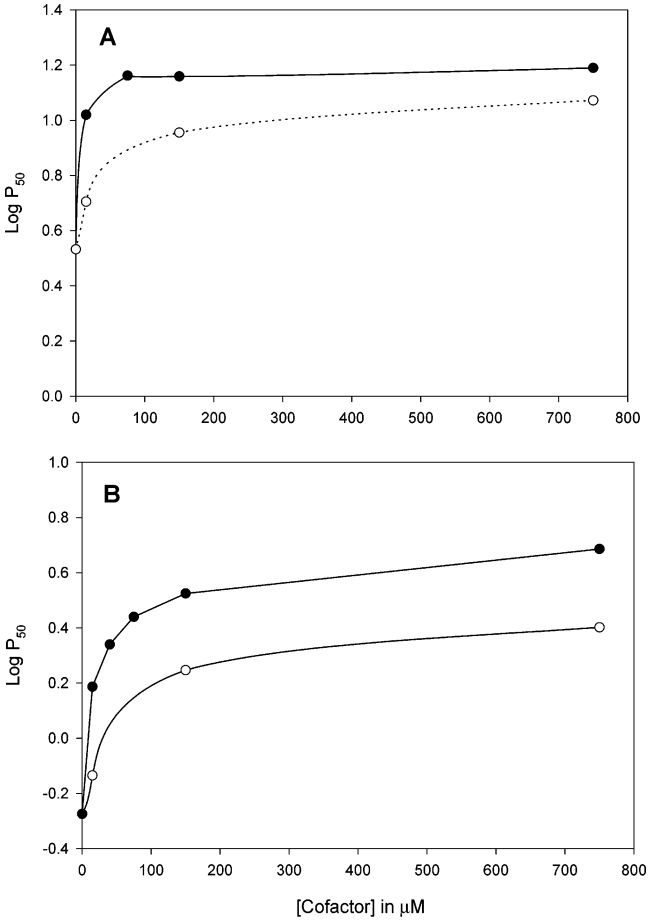

FIGURE 7: Effects of PyTS on oxygen binding by Hb A. Effects of PyTS and DPG on oxygen binding curves at pH 6.5 (A) and 7.5 (B). Solution conditions were 60 μM Hb A at pH 7.5 in 0.05 M Bis-Tris buffer at 20 °C with DPG (●) or PyTS (○).

weaker nonspecific anion binding sites. Notably, although PyTS is a polyvalent ionic effector, at a 1:1 effector:tetramer ratio, it decreases oxygen affinity only ~25% as much as DPG does (at both pH 6.5 and 7.5). At pH 6.5, a 1:1 PyTS:Hb tetramer ratio brings about only ~50% of the shift observed when the effector concentration is increased 50-fold. Similar differences are apparent at pH 7.5. Because the highest-affinity binding of PyTS to the tetramer can be confidently ascribed to its polyionic binding to the DPG binding site, we were able to examine the effects of ligation and competitive ions on the DPG binding site by examination of competitive effects when PytS was present at the low 1:1 effector:tetramer ratio.

Changes in PyTS Fluorescence upon Addition of Other Effectors. The following paragraphs describe in detail the changes in PyTS emission upon addition of IHP, L35, and Cl^- to both the CO and deoxy Hb A derivatives at pH 6.5, 7.5, and 8. Figure 8 shows several representative PyTS fluorescence spectra that illustrate the pattern of intensity change occurring with the sequential addition of effectors to a 1:1 PyTS/CO Hb A sample at pH 6.5. Table 1 summarizes the fractional changes in the PyTS intensity for CO Hb A, deoxy Hb A, and sol−gel-encapsulated CO Hb A at pH 6.5. Figure 9 shows these and the relative changes in additional samples in graphical form. In both Table 1 and Figure 9, the relative PyTS emission intensity is normalized to the signal observed for the 1:1 PyTS/CO Hb A sample at

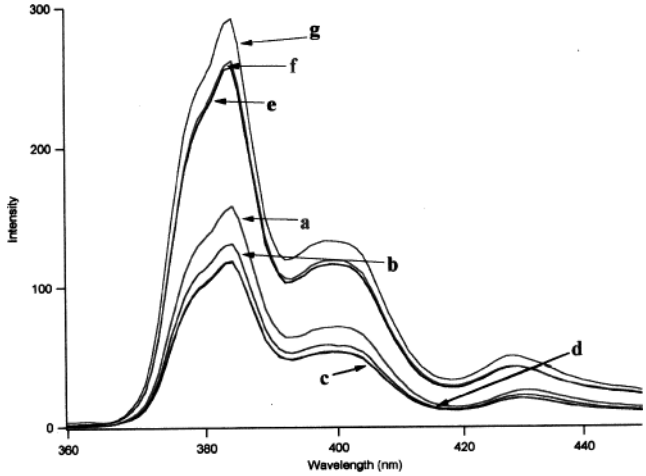

FIGURE 8: Effector-induced changes in the fluorescence spectrum of a 1:1 PyTS/CO Hb A tetramer solution (Hb at 0.5 mM in heme) at room temperature. Traces correspond to the following effector: Hb tetramer ratios: (a) no additions, (b) L35 at 2:1, (c) L35 at 4:1, (d) L35 at 6:1, (e) L35 at 6:1 and IHP at 2:1, (f) L35 at 6:1 and IHP at 4:1, and (g) L35 at 6:1, IHP at 4:1, and Cl^- at 1000:1.

Table 1: Fractional Change in the Front Face Fluorescence Intensity of PyTS in a 1:1 PyTS/Hemoglobin Solution (pH 6.5) as a Function of Added Effectors and Corresponding Percentage of Bound PyTS in Parenthses[a]

added effector	CO Hb A	deoxy Hb A	[CO Hb A]
PyTS	1.0 (87)	1.0 (87)	1.0 (87)
PyTS and Cl^-	2.5 (54)	1.7 (72)	0.85 (90)
PyTS and IHP	2.1 (63)	1.5 (76)	1.6 (74)
PyTS and L35	0.7 (93)	0.5 (98)	
PyTS, IHP, and Cl^-	2.8 (48)		1.4 (78)
PyTS, IHP, and L35	1.6 (74)	1.1 (85)	1.0 (87)
PyTS, IHP, L35, and Cl^-	1.8 (70)	1.3 (80)	0.6 (96)

[a] All values are referenced to the 1:1 PyTS/CO Hb A emission intensity. In each case, the value is for the sample under conditions where the maximum effect is observed. The bracket notation refers to a sample encapsulated in a porous sol−gel matrix that is immersed in buffer (pH 6.5).

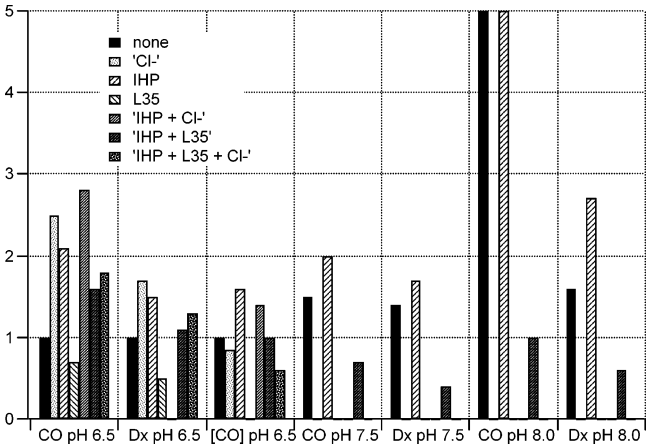

FIGURE 9: Summary of effector-induced changes in the fluorescence spectra of a 1:1 PyTS/Hb A tetramer sample (samples in solution and in a sol−gel matrix).

pH 6.5. The values are the end point values, representing the maximum change occurring for a given combination of added effectors. The solution-phase results can be summarized as follows. For both the CO and deoxy derivatives, the addition of IHP (in slight excess over the tetramer concentration) or Cl^- (in large excess) increases the mag-

nitude of the fluorescence signal from PyTS, whereas the addition of L35 decreases the fluorescence in both the absence and presence of IHP or Cl^-. The IHP effect decreases with increasing pH, with the pH dependence being much greater for the CO derivative. The L35 effect exhibits a minimal dependence upon pH.

PyTS Fluorescence of Sol−Gel-Encapsulated CO Hb A at pH 6.5. Addition of IHP and L35 (alone and in combination) to a pH 6.5 sol−gel-encapsulated 1:1 PyTS/CO Hb A sample produced results similar to those observed in solution. IHP enhances the fluorescence, with a maximum change of approximately 60% for IHP at 5:1 (Table 1, relative intensity of ~1.6). The subsequent addition of L35 appears to exactly offset the IHP-induced enhancement (relative intensity of 1). Whether the expected amount of effector enters the gel pores remains an open question, but this agreement with the solution results strongly indicates that with a sufficient equilibration time the anticipated effector:tetramer ratio is achieved.

Remarkably, when Cl^- is added to the sol−gel samples, the fluorescence intensity decreases. This result is opposite in direction to that observed for samples in solution where the addition of Cl^- always increases the fluorescence intensity. This behavior contrasts to effects observed for IHP and L35, which induce a similar PyTS response in solution and sol−gel samples. The addition of 0.6 M Cl^- to an IHP- and L35-free sample of CO Hb A at pH 6.5 resulted in an immediate and persistent reduction of the fluorescence intensity on the order of 15% (relative intensity of 0.85). A similarly sized decrease occurred when addition of 0.6 M Cl^- was made to a sample containing IHP at 6:1 relative to Hb tetramer (relative intensity of 1.4). The addition of 0.06 M Cl^- to a sample containing both IHP and L35 at 6:1 produced a much smaller reduction in fluorescence (on top of the reduction induced by adding L35 to the IHP-treated sample). Overall, it appears that for the sol−gel samples, the addition of a large excess of Cl^- mimics the behavior brought about by addition of stoichiometric amounts of L35.

DISCUSSION

PyTS Is an Allosteric Effector. The effect of PyTS on binding of oxygen to Hb A is clearly like that of DPG, implying that it too stabilizes the low-affinity T-state conformation of Hb. This is an expected result, since the PyTS structure is in many ways analogous to DPG and other anionic effectors that have been shown to bind in a 1:1 effector:deoxy Hb ratio at a positively charged site between the two β chains (*6*, *7*). The pH-dependent PyTS effect on oxygen binding is also consistent with a progressively larger difference in PyTS binding affinity between deoxy and liganded Hb at higher pH, as reflected in the fluorescence intensity changes reported in this paper.

Because the highest-affinity binding of PyTS to the tetramer is plausibly ascribed to its polyionic binding to the DPG binding site or $\beta\beta$ cleft, we were able to examine the effects of ligation and competitive ions on the DPG binding site by examining the effects when PyTS was present at a 1:1 effector:tetramer ratio. Support for this assertion regarding the DPG binding site comes from our very recent studies (manuscript in preparation) on Hb with an electrostatic modification of the $\beta\beta$ cleft caused by 3-phospho-2-hydroxypropylation of Val1β. This modified Hb (to be termed G3P-Hb A) is IHP insensitive with respect to oxygen binding and shows little or no binding of PyTS (both CO and deoxy derivatives) with the PyTS fluorescence showing no change upon addition of either IHP or Cl^- to a 1:1 mixture of G3P-Hb and PyTS. The conclusion from these findings is that under the conditions employed in this study, PyTS occupies the DPG binding site of Hb A.

Effect of Ligation State on Binding of PyTS to Hb A. As in a previous study (*38*), we have observed herein that in general PyTS binds more effectively to deoxy Hb A than to ligated Hb A, which underlies its ability to act as an allosteric effector and lower oxygen affinity. This preferential binding to the deoxy state is pH-dependent, with both ligated and unligated states showing a decrease in the level of PyTS binding with increasing pH, as expected due to partial deprotonation of residues in the DPG binding site at high pH. The difference in PyTS binding affinity between deoxy and CO-ligated Hb is close to zero at pH 6.5 but becomes progressively larger at higher pH so that by pH 8 no binding is seen for the CO derivative, as reflected in the fluorescence intensities.

IHP and Cl^- Competitively Inhibit Binding of PyTS to Hb in Solution. The addition of either IHP or Cl^- to the 1:1 solution of PyTS and Hb (deoxy or CO) results in an increase in PyTS fluorescence, indicative of an increase in the relative concentration of free PyTS as it is being displaced at the DPG site by IHP. This result is consistent with the earlier proposal that the DPG binding site is the strong binding site for PyTS (*38*) and the recent results cited above regarding the absence of PyTS binding for G3P-Hb A.

IHP Exhibits a Self-Competition Effect when Added to CO Hb A. Addition of stoichiometric amounts of IHP to CO Hb A at pH values between 7 and 6 results in a decrease in the geminate yield and a decrease in the frequency of ν(Fe−His) in the nanosecond photoproduct Raman spectrum. On the basis of the PyTS results, it can be assumed that at these concentrations, the IHP is binding to the DPG binding site despite the ligation status of the sample.

Increases in the IHP concentration above a ratio of 10:1 relative to the Hb tetramer result in a complete reversal of the changes in the geminate yield and the Raman spectrum such that they very nearly have the same values as when no IHP is bound. The simplest explanation for this effect is that the high-affinity binding site for IHP is still the DPG binding site, despite the ligation status of the Hb A, but that there are also weaker IHP binding sites that only become populated when there is an appreciable amount of IHP present in an excess of the tetramer concentration. It should be noted that the changes in Raman spectra and the geminate yield under conditions of excess IHP are not consistent with IHP inducing extensive dimer formation (*23*, *60*). The high concentration of CO Hb also precludes the possibility that high IHP levels are creating a large population of dimers, which is seen to occur at much lower Hb concentrations (*61*−*63*).

A recent X-ray crystallographic study (*64*) indicates that the narrowed R-state $\beta\beta$ cleft still is sufficiently flexible to accommodate the binding of DPG-type effectors. This study shows that phosphates can bind to the DPG site in fully ligated R-state Hb. The reported structure also reveals perturbations to the R structure required to expand the normally narrow R-state $\beta\beta$ cleft. These type of changes,

which are in the direction of the R to T quaternary transition, are likely to be responsible for the changes reflected in the IHP-induced (and phosphate, E. S. Peterson, U. Samuni, and J. M. Friedman, unpublished results) reduction in GY and Raman frequency reported in this and previous studies. These results support the notion that there is sufficient plasticity within the R structure to accommodate binding of effectors at the DPG binding site. Plasticity within the DPG site within the T state has also been observed (*65*). In this instance, the overall T-state conformation is retained despite progressive narrowing of the $\beta\beta$ cleft in the deoxy Hb derivative due to different lengths of a cross-linker between the two Lys82β residues.

The self-induced loss of the kinetic and spectroscopic signatures of binding of IHP to the $\beta\beta$ cleft in CO Hb A at high IHP concentrations can possibly be explained by the eventual binding of IHP at its lower-affinity sites as more IHP is added to the solution. Potential candidates for these additional sites are sites within the central cavity other than the DPG site at the $\beta\beta$ cleft. Binding of IHP to its low-affinity site could alter binding at the strong binding site due to strong repulsive electrostatic interactions between the DPG site IHP molecules and the loosely bound central cavity-bound IHP. Alternatively, the binding of IHP to the weaker site (or occupancy in the central cavity without a specific well-defined binding site) could induce a heretofore undetected conformational change in the central cavity that increases the energy cost of binding of IHP to the $\beta\beta$ cleft. As discussed in the next paragraphs, the L35 results support ascribing the weaker IHP sites to the central cavity.

L35 Enhances PyTS Binding. Unlike IHP, L35 does not reduce the level of PyTS binding for either deoxy or fully ligated Hb A between pH 6.5 and 8. Addition of L35 always decreases the PyTS emission no matter what other effectors are present, indicating that L35 binding increases the affinity of PyTS for the $\beta\beta$ cleft site. Other studies have indicated that bezafibrate-type effectors enhance the allosteric impact of DPG site effectors (*66*, *67*). The absence of competition between PyTS and L35 is also in accord with the crystallographic studies on deoxy Hb A (*5*−*7*) showing that L35 occupies sites within the central cavity that are distinct from the $\beta\beta$ cleft where DPG, IHP, and PyTS all bind. For L35 (*5*), there is in addition to this primary strong binding site (*68*−*70*), a secondary site that extends toward but does not quite reach the $\beta\beta$ cleft DPG site. It is not yet clear what role, if any, this secondary site plays in modulating Hb reactivity. The enhanced binding of PyTS upon addition of L35 indicates that the occupancy by L35 of some or all of these potential binding sites within the central cavity results in a more favorable PyTS binding site at the $\beta\beta$ cleft of the central cavity. These potential L35 binding sites are discussed further below in light of the combined effects of L35 and IHP.

L35 Partially Reverses the Effect of Cl^- on PyTS Binding. The partial reversal of the Cl^- effect (reduced level of PyTS binding in the presence of Cl^-) by L35 likely results from two effects. The first discussed above is that L35 makes the DPG binding site more favorable for the binding of PyTS. The second proposed effect is L35 effectively competing with Cl^- for occupancy within the central cavity. The displacement of PyTS by the large excess of Cl^- likely arises from the presence of Cl^- not only at the DPG binding site proper but also via more long-range electrostatic interactions from Cl^- ions loosely localized in the central cavity near the DPG binding site (*71*, *72*). It is probable that L35 displaces the negatively charged chloride ions from the central cavity sites distal to the DPG site. As a result, the longer-range electrostatic repulsive interactions between Cl^- and PyTS would be reduced.

L35 Reduces the Effect of IHP on PyTS Binding and Reverses the Self-Competition Effect of IHP. This study shows that binding of L35 preferentially enhances the affinity of PyTS for the $\beta\beta$ cleft over that of IHP as evidenced by the weakened ability of IHP to displace PyTS when L35 is present. Evidence that L35 exerts an effect on the DPG binding site in CO Hb A from "below" also follows from the observed effects of IHP and L35 on both the geminate recombination and photoproduct Raman spectra. The addition of L35 to a sample containing a 20:1 IHP:Hb tetramer ratio results in the elimination of the IHP self-competition effect and concomitant reappearance of a reduced geminate yield and ν(Fe−His) frequency. The most straightforward explanation for the loss of the IHP self-inhibitory effect through the addition of L35 is that L35 binds in sites that interfere with IHP binding in its low-affinity sites. As discussed above, it is the presence of IHP in these secondary sites that is proposed to be the cause of the self-inhibitory effect. It is possible that these sites are the same or in the proximity of each other, in which case they are both likely within the central cavity since this is where several L35 sites have been found (*vide supra*). Synergistic effects between bezafibrate-type molecules (including L35) and IHP have been previously reported (*5*, *66*, *67*, *73*) and adduced as evidence supporting long-range communication within the central cavity. Also consistent with this picture is the recent report of calorimetric measurements showing evidence for one strong and two weak IHP binding sites on CO Hb A and showing that the presence of L35 eliminates one of the weak sites (*74*).

L35 Binding Site in CO Hb A. The similarity in the results of the CO Hb A and deoxy Hb A competition experiments with L35, IHP, PyTS, and Cl^- suggests that L35 exerts its influence via the same pathway for both unligated and ligated Hb. The behavior of L35 is most easily explained in terms of a model in which it binds within the central caity. While the X-ray data clearly indicate that L35 binds within the central cavity of deoxy Hb A, there are not such structural data for the ligated derivative. Indeed, a recent X-ray crystallographic study revealed bezafibrate binding to sites on CO Hb (horse) external to the central cavity (*75*). Given the similarity in how L35 affects binding of PyTS to deoxy and CO Hb A, it seems implausible that the same effect could arise from L35 binding to either of two very different sites. The UV resonance Raman data presented herein support interpretations in which L35 binds in the central cavity in both instances.

X-ray crystallographic studies reveal that there is a well-defined binding site in deoxy Hb A toward the $\alpha\alpha$ end of the central cavity for L35 (*5*), bezafibrate (*8*), and other bezafibrate-type effectors (*68*−*70*, *76*, *77*). Several key interactions are evident between L35 and residues in its primary binding site in the α end of the central cavity. Two of these contacts in the deoxy structure can account for the observed L35-induced changes in the UV resonance Raman

spectrum of CO Hb A and are therefore also presumed to be present for L35 bound in ligated Hb. The first of these contacts involves the methylpropionic acid moiety of L35 which is in position to hydrogen bond with Arg141α. The reduction in oxygen affinity associated with the binding of these bezafibrate-type effectors is attributed to the stabilization of the interactions of the C-terminus of the α subunits as can be seen in reduced *B* factors for Tyr140α and Arg141α (*69*). For the T state, the reduced mobility of Tyr140α has been directly linked both to the stability of the hinge region of the $\alpha_1\beta_2$ interface (*78*) and to the degree of proximal strain at the heme of the α subunits, which in turn is directly related to the ligand binding barrier (*23*, *79*). The L35-induced intensity change observed in the tyrosine Y8a Raman band likely reflects the linked response of Tyr140α and Arg141α arising from the latter residue's hydrogen bonding to L35. This interaction in turn results in stronger hydrogen bonding between the phenolate proton of Tyr140α and the carbonyl of Val93α due to the greater stability in this region upon L35 binding (*vide infra*). The non-central cavity binding site observed for bezafibrate in crystals of horse COHb cannot account for the observed spectroscopic changes in any obvious fashion.

The second relevant contact between L35 and the central cavity involves a hydrophobic contact between the phenoxy ring of L35 and Trp37*β*, which explains the intensity changes seen in the low-frequency shoulder of the W3 band. This intensity change is also seen for deoxy Hb A and half-ligated derivatives of Fe−Zn hybrids of Hb A (*80*).

In the αα cross-linked CO Hb A, the fumaryl cross-linker between the two Lys99α residues results in the loss of the L35-induced intensity change in the tyrosine Y8a band attributed to Tyr140α, but the changes seen in the W3 band remain. The carbonyl in the center of the L35 effector hydrogen bonds with the amino side chain of Lys99α. The interaction with Lys99α is viewed as being critical for stabilizing this class of effectors in their primary binding site (*77*). There are two plausible explanations for the changes in the UVRR spectrum due to the cross-linker. One possibility is that the cross-linker alters the primary binding site located in the region of residue 99α in a manner that does not prevent L35 binding (hence the change in W3) but does prevent or precludes the hydrogen bonding of L35 to Arg141α and therefore eliminates the changes in the Y8a bands. Alternatively, the cross-link may directly stabilize the hydrogen binding between Tyr140α and Val93α so that further stabilization of this region upon binding of L35 does not occur. Evidence for this latter interpretation is apparent in the increased Tyr Y8a intensity in the cross-linked Hb spectrum relative to that seen in the native spectrum (Figure 6). Furthermore, a previous UVRR study (*81*) showed a direct coupling between interactions affecting Lys99α and intensity changes in Y8a. A convincing argument was made that these intensity changes arose from modulation of the hydrogen binding between Tyr140α and Val93α through interactions associated with α99.

Summary of the L35 Mechanism. Earlier studies have shown that IHP and bezafibrate-type effectors such as L35 act synergistically with respect to oxygen affinity (*5*, *8*, *15*, *47*, *66*). Both effectors independently affect ligated Hb A as reflected in the reduction in the geminate yield and in the frequency of *ν*(Fe−His) for the CO Hb A photoproduct, indicating that earlier conclusions regarding the two effectors clearly extend to the properties of fully ligated Hb A. These results support the assertion that the L35-enhanced binding of PyTS to CO Hb A is in part due to a perturbation of the ligated Hb A structure that makes the DPG binding site more accessible to DPG site effectors and the protein more responsive to these effectors. Despite the reduction in the volume of the R-state central cavity, the data are most consistent with a picture in which L35 interacts with the central cavity of both T- and R-state family members. The L35, by virtue of occupying (or otherwise affecting) the central cavity, might actually induce an increase in the overall volume of the R-state central cavity that facilitates binding at the *ββ* cleft. The synergistic effects with IHP may also result from the specific interactions between L35 and the residues lining the central cavity. The individual effects of L35 on the geminate yield and the Fe−His stretching frequency are likely to be the direct consequence of the interactions linking L35, Arg141α, and Tyr140α as well as Trp37*β*, all of which influence the proximal response at the heme of the α subunit in a manner that reduces ligand affinity.

In contrast to the situation with CO Hb A, the addition of L35 does not perturb the frequency of *ν*(Fe−His) for the deoxy T state (data not shown). The recently published high-resolution X-ray study of deoxy Hb A with an L35-like effector localized within the central cavity reveals that the overall quaternary and tertiary structure of deoxy Hb A is not altered; however, as described above, L35 does impart greater stability to several functionally important domains within the globin (*69*). These results support the premise that L35 enhances binding of PyTS to deoxy Hb A at pH 6.5 by stabilizing conformational substates within the T quaternary structure that bind DPG-type effectors more tightly. This conjecture is also consistent with our recent observations that L35 is very effective (much more so than IHP) in slowing the conformational evolution of the deoxy T-state structure for sol−gel-encapsulated deoxy Hb A upon addition of CO (U. Samuni, D. Dantsker, L. Juszczak, and J. M. Friedman, unpublished results). Alterations in the distribution of thermally accessible conformational substates have previously been invoked to account for the effect of Cl^- on both the T-state ligand binding and T-state reactivity of the 93*β* sulfhydryl group (*1*).

Binding of PyTS to Sol−Gel-Encapsulated Hb A. Encapsulation of proteins in porous sol−gel matrices offers the promise of being able to add and remove potentially interactive substrates and study their interaction with both equilibrium and nonequilibrium forms of Hb A. This study shows that studies of effector binding to sol−gel-encapsulated Hb are feasible and informative. The results show that care must be given to allow for the equilibration of added anions into the sol−gel matrix. Earlier diffusion studies (*82*−*84*) revealed that appropriately sized cations and neutral solvent soluble molecules can diffuse into porous sol−gel matrices at rates indicative of free diffusion, whereas anions diffuse more slowly, presumably due to the excess negative charge associated with the sol−gel polymers. This study clearly demonstrates that anionic effectors can diffuse through the sol−gel matrix (albeit slowly) and access encapsulated Hb.

Anomalous Cl^- Effect for Sol−Gel-Encapsulated Hb A. The properties of binding of PyTS to deoxy Hb A and CO Hb A as a function of pH in solution are also seen in the corresponding sol−gel-encapsulated samples. The IHP and L35 effects observed in solution are similarly manifested in the sol−gel matrix. The single seemingly anomalous observation is the increase in the level of PyTS binding with the addition of Cl^- to both IHP-free and IHP-bound samples of encapsulated Hb A.

A possible explanation for this solution versus gel difference in the Cl^- effect might be based on the limited solvation volume surrounding encapsulated proteins (*53*, *82*, *85*). As the sol−gel matrix forms, the growing polymers form a template around the protein. The end result is a relatively tight fitting cage around each protein molecule. Although the protein still retains a hydration shell, the limited volume may preclude the presence of a high concentration of solvated ions within the restricted volume. The solution-phase effect in which Cl^- displaces PyTS was proposed to be due to an electrostatic shielding of the DPG binding site by a large excess of Cl^- on the surface of the protein and within the central cavity. Through both the reduction in the available volume and the negative polarity of the different Si−O moieties that line the pores of the sol−gel matrix, we propose that the sol−gel matrix reduces the surface population of Cl^- but has little effect on the population of Cl^- situated within the central cavity. In this scenario, Cl^- loses its efficacy on the surface but retains its "internal" effects. With the reduction of the surface effect, Cl^- may behave more like L35 and thus enhance PyTS binding at both high and low pH values through a central cavity-induced conformational change at the $\beta\beta$ cleft that then strengthens PyTS binding. In addition, it can be argued, purely on the basis of the electrostatic consideration, that the presence of an excess of negative charge within the central cavity but not on the surface should preferentially reduce the level of IHP binding at the DPG binding site with respect to PyTS given the added anionic groups on IHP.

CONCLUSIONS

These results support the growing body of literature showing that allosteric effectors not only shift the equilibrium between quaternary states but also directly perturb the functional and conformational properties of the individual quaternary states. Furthermore, it is apparent that the central cavity of Hb A is capable of supporting a spectrum of allosteric interactions, including both synergistic and competitive effects that seemingly arise from relatively long-range communication pathways mediated by reactions within the cavity, including effector binding, covalent cross-linking, and nonspecific binding of anions. In particular, the observation that L35 enhances PyTS binding indicates that PyTS can be used to rapidly compare different bezafibrate-type effectors with respect to central cavity interactions and thereby help expose those elements of structure that are responsible for such effects.

How T−R intermediate states of Hb A, such as possible transition-state species, respond to allosteric effectors is an important element in establishing the detailed mechanisms associated with allostery. In this study, sol−gel encapsulation of Hb A, a method for the trapping of nonequilibrium states, was used in combination with PyTS to explore the feasibility of probing the binding of an effector to sol−gel-encapsulated species. The results clearly indicate that the solution-phase protocols associated with the use of PyTS can be extended to sol−gel matrices. PyTS, IHP, and L35 bring about effects in the sol−gel-encapsulated Hb that are similar to effects observed in solution. In contrast, Cl^- exhibits a complete reversal of behavior in the gels. In solution, Cl^- displaces PyTS, whereas in the sol−gel samples, it behaves like L35, as reflected in its enhancement of the binding of PyTS to Hb A. It is proposed that this new effect stems from the sol−gel matrix limiting the concentration of Cl^- on the surface of Hb but not in the interior of the central cavity. By eliminating the surface effects that dominate the solution-phase studies, the sol−gel matrix allows exposure of the more subtle anionic effects arising from the central cavity of Hb A.

Several of the proposed mechanisms that most directly account for the observed competitive and synergistic behavior of added effectors on the functional and conformational properties of ligated Hb A are in conflict with much of the X-ray crystallographic data from ligated Hb A. The structural data imply that the dimensions of the central cavity, including the $\beta\beta$ cleft, are not adequate for accommodating effector binding. This seeming conflict raises important questions about what functionally important dynamical features of a protein are likely to be missed in the crystal studies that likely examine one of possibly many conformations accessed in solution under equilibrium conditions.

REFERENCES

1. Bonaventura, C., Tesh, S., Faulkner, K. M., Kraiter, D., and Crumbliss, A. L. (1998) Conformational fluctuations in deoxy hemoglobin revealed as a major contributor to anionic modulation of function through studies of the oxygenation and oxidation of hemoglobins A0 and Deer Lodge β2(NA2)His → Arg, *Biochemistry 37*, 496−506.
2. Yonetani, T., Park, S. I., Tsuneshige, A., Imai, K., and Kanaori, K. (2002) Global allostery model of hemoglobin. Modulation of O(2) affinity, cooperativity, and Bohr effect by heterotropic allosteric effectors, *J. Biol. Chem. 277*, 34508−34520.
3. Tsuneshige, A., Park, S., and Yonetani, T. (2002) Heterotropic effectors control the hemoglobin function by interacting with its T and R states: a new view on the principle of allostery, *Biophys. Chem. 98*, 49−63.
4. Imai, K., Tsuneshige, A., and Yonetani, T. (2002) Description of hemoglobin oxygenation under universal solution conditions by a global allostery model with a single adjustable parameter, *Biophys. Chem. 98*, 79−91.
5. Lalezari, I., Lalezari, P., Poyart, C., Marden, M., Kister, J., Bohn, B., Fermi, G., and Perutz, M. F. (1990) New effectors of human hemoglobin: structure and function, *Biochemistry 29*, 1515−1523.
6. Arnone, A. (1972) X-ray diffraction study of binding of 2,3-diphosphoglycerate to human deoxyhaemoglobin, *Nature 237*, 146−149.
7. Arnone, A., and Perutz, M. F. (1974) Structure of inositol hexaphosphate−human deoxyhaemoglobin complex, *Nature 249*, 34−36.
8. Perutz, M. F., and Poyart, C. (1983) Bezafibrate lowers oxygen affinity of haemoglobin, *Lancet 2*, 881−882.
9. Alpert, B., El Mohsni, S., Lindqvist, J., and Tfibel, F. (1979) Transient effects in the nanosecond laser photolysis of carboxyhemoglobin:cage recombination and spectral evolution of the protein, *Chem. Phys. Lett.*, 11−16.
10. Duddell, D. A., Morris, R. J., Muttucumaru, N. J., and Richards, J. T. (1980) The dependence of the quantum yield of ligand photodissociation from haem proteins on ultrafast recombination, *Photochem. Photobiol. 11*, 479−484.

11. Friedman, J. M., and Lyons, K. B. (1980) Transient Raman study of CO-haemoprotein photolysis: origin of the quantum yield, *Nature 284*, 570−572.
12. Findsen, E. W., Friedman, J. M., Ondrias, M. R., and Simon, S. R. (1985) Picosecond time-resolved resonance Raman studies of hemoglobin: implications for reactivity, *Science 229*, 661−665.
13. Friedman, J. M., Scott, T. W., Fisanick, G. J., Simon, S. R., Findsen, E. W., Ondrias, M. R., and Macdonald, V. W. (1985) Localized control of ligand binding in hemoglobin: effect of tertiary structure on picosecond geminate recombination, *Science 229*, 187−190.
14. Marden, M. C., Hazard, E. S., Kimble, C., and Gibson, Q. H. (1987) Geminate ligand recombination as a probe of the R, T equilibrium in hemoglobin, *Eur. J. Biochem. 169*, 611−615.
15. Marden, M. C., Kister, J., Bohn, B., and Poyart, C. (1988) T-state hemoglobin with four ligands bound, *Biochemistry 27*, 1659−1664.
16. Hofrichter, J., Henry, E. R., Sommer, J. H., Deutsch, R., Ikeda-Saito, M., Yonetani, T., and Eaton, W. A. (1985) Nanosecond optical spectra of iron−cobalt hybrid hemoglobins: geminate recombination, conformational changes, and intersubunit communication, *Biochemistry 24*, 2667−2679.
17. Khan, I., Dantsker, D., Samuni, U., Friedman, A. J., Bonaventura, C., Manjula, B., Acharya, S. A., and Friedman, J. M. (2001) β93 modified hemoglobin: kinetic and conformational consequences, *Biochemistry 40*, 7581−7592.
18. Khan, I., Shannon, C. F., Dantsker, D., Friedman, A. J., Perez-Gonzalez-de-Apodaca, J., and Friedman, J. M. (2000) Sol−gel trapping of functional intermediates of hemoglobin: geminate and bimolecular recombination studies, *Biochemistry 39*, 16099−16109.
19. Abbruzetti, S., Viappiani, C., Bruno, S., Bettati, S., Bonaccio., M., and Mozzarelli, A. (2001) Functional characterization of heme proteins encapsulted in wet nanoporous silica gels, *J. Nanosci. Nanotechnol. 1*, 407−413.
20. Friedman, J. M., Rousseau, D. L., Ondrias, M. R., and Stepnoski, R. A. (1982) Transient Raman study of hemoglobin: structural dependence of the iron-histidine linkage, *Science 218*, 1244−1246.
21. Friedman, J. M., Scott, T. W., Stepnoski, R. A., Ikeda-Saito, M., and Yonetani, T. (1983) The iron-proximal histidine linkage and protein control of oxygen binding in hemoglobin. A transient Raman study, *J. Biol. Chem. 258*, 10564−10572.
22. Friedman, J. M. (1985) Structure, dynamics, and reactivity in hemoglobin, *Science 228*, 1273−1280.
23. Peterson, E. S., and Friedman, J. M. (1998) A possible allosteric communication pathway identified through a resonance Raman study of four β37 mutants of human hemoglobin A, *Biochemistry 37*, 4346−4357.
24. Rousseau, D. L., and Friedman, J. M. (1988) in *Biological Applications of Raman Spectroscopy* (Spiro, T. G., Ed.) pp 133−215, John Wiley & Sons, New York.
25. Kitagawa, T. (1988) in *Biological Application of Raman Spectroscopy* (Spiro, T. G., Ed.) pp 97−131, John Wiley & Sons, New York.
26. Friedman, J. M. (1994) Time-resolved resonance Raman spectroscopy as probe of structure, dynamics, and reactivity in hemoglobin, *Methods Enzymol. 232*, 205−231.
27. Jayaraman, V., Rodgers, K. R., Mukerji, I., and Spiro, T. G. (1995) Hemoglobin allostery: resonance Raman spectroscopy of kinetic intermediates, *Science 269*, 1843−1848.
28. Samuni, U., Dantsker, D., Khan, I., Friedman, A. J., Peterson, E., and Friedman, J. M. (2002) Spectroscopically and kinetically distinct conformational populations of sol−gel-encapsulated carbonmonoxy myoglobin. A comparison with hemoglobin, *J. Biol. Chem. 277*, 25783−25790.
29. Ondrias, M. R., Rousseau, D. L., Shelnutt, J. A., and Simon, S. R. (1982) Quaternary-transformation-induced changes at the heme in deoxyhemoglobins, *Biochemistry 21*, 3428−3437.
30. Ondrias, M. R., Rousseau, D. L., Kitagawa, T., Ikeda-Saito, M., Inubushi, T., and Yonetani, T. (1982) Quaternary structure changes in iron−cobalt hybrid hemoglobins detected by resonance Raman scattering, *J. Biol. Chem. 257*, 8766−8770.
31. Friedman, J. M., Rousseau, D. L., Ondrias, M. R., and Stepnoski, R. A. (1982) Transient Raman study of hemoglobin: structural dependence of the iron−histidine linkage, *Science 218*, 1244−1246.
32. Huang, J., Juszczak, L. J., Peterson, E. S., Shannon, C. F., Yang, M., Huang, S., Vidugiris, G. V., and Friedman, J. M. (1999) The conformational and dynamic basis for ligand binding reactivity in hemoglobin Ypsilanti (β99 Asp → Tyr): origin of the quaternary enhancement effect, *Biochemistry 38*, 4514−4525.
33. Hu, X., Rodgers, K. R., Mukerji, I., and Spiro, T. G. (1999) New light on allostery: dynamic resonance Raman spectroscopy of hemoglobin kempsey, *Biochemistry 38*, 3462−3467.
34. MacQuarrie, R., and Gibson, Q. H. (1972) Ligand binding and release of an analogue of 2,3-diphosphoglycerate from human hemoglobin, *J. Biol. Chem. 247*, 5686−5694.
35. Marden, M. C., Hazard, E. S., and Gibson, Q. H. (1986) Testing the two-state model: anomalous effector binding to human hemoglobin, *Biochemistry 25*, 7591−7596.
36. Gottfried, D. S., Juszczak, L. J., Fataliev, N. A., Acharya, A. S., Hirsch, R. E., and Friedman, J. M. (1997) Probing the hemoglobin central cavity by direct quantification of effector binding using fluorescence lifetime methods, *J. Biol. Chem. 272*, 1571−1578.
37. Serbanescu, R., Kiger, L., Poyart, C., and Marden, M. C. (1998) Fluorescent effector as a probe of the allosteric equilibrium in methemoglobin, *Biochim. Biophys. Acta 1363*, 79−84.
38. Gottfried, D. S., Manjula, B. N., Malavalli, A., Acharya, A. S., and Friedman, J. M. (1999) Probing the diphosphoglycerate binding pocket of HbA and HbPresbyterian (β108Asn → Lys), *Biochemistry 38*, 11307−11315.
39. Shibayama, N., and Saigo, S. (1995) Fixation of the quaternary structures of human adult haemoglobin by encapsulation in transparent porous silica gels, *J. Mol. Biol. 251*, 203−209.
40. Bettati, S., and Mozzarelli, A. (1997) T state hemoglobin binds oxygen noncooperatively with allosteric effects of protons, inositol hexaphosphate, and chloride, *J. Biol. Chem. 272*, 32050−32055.
41. Das, T. K., Khan, I., Rousseau, D. L., and Friedman, J. M. (1999) Temperature-dependent quaternary state relaxation in sol−gel encapsulated hemoglobin, *Biospectroscopy 5*, S64−S70.
42. Juszczak, L. J., and Friedman, J. M. (1999) UV resonance Raman spectra of ligand binding intermediates of sol−gel encapsulated hemoglobin, *J. Biol. Chem. 274*, 30357−30360.
43. Acharya, A. S., Sussman, L. G., and Manning, J. M. (1983) Schiff base adducts of glyceraldehyde with hemoglobin. Differences in the Amadori rearrangement at the α-amino groups, *J. Biol. Chem. 258*, 2296−2302.
44. Chatterjee, R., Welty, E. V., Walder, R. Y., Pruitt, S. L., Rogers, P. H., Arnone, A., and Walder, J. A. (1986) Isolation and characterization of a new hemoglobin derivative cross-linked between the α chains (lysine 99 α 1−lysine 99 α 2), *J. Biol. Chem. 261*, 9929−9937.
45. Juszczak, L. J., Manjula, B., Bonaventura, C., Acharya, S. A., and Friedman, J. M. (2002) UV resonance Raman study of β93-modified hemoglobin A: chemical modifier-specific effects and added influences of attached poly(ethylene glycol) chains, *Biochemistry 41*, 376−385.
46. Campbell, B. F., Magde, D., and Sharma, V. S. (1984) Geminate recombination in carboxy hemoglobin A and its relation to overall carbon monoxide reactivity, *J. Mol. Biol. 179*, 143−150.
47. Marden, M. C., Bohn, B., Kister, J., and Poyart, C. (1990) Effectors of hemoglobin. Separation of allosteric and affinity factors, *Biophys. J. 57*, 397−403.
48. Scott, T. W., Friedman, J. M., and Macdonald, V. W. (1985) Distal and Proximal Control of Ligand Reactivity: A Transient Raman Comparison of COHbA and COHb (Zurich), *J. Am. Chem. Soc. 107*, 3702−3705.
49. Zhao, X., Chen, R., Raj, V., and Spiro, T. G. (2001) Assignment of the 1511 cm^{-1} UV resonance Raman marker band of hemoglobin to tryptophan, *Biopolymers 62*, 158−162.
50. Su, C., Park, Y. D., Liu, G., and Spiro, T. G. (1989) Hemoglobin T−R Structure Dynamics from Simltaneous Monitoring of Tyrosine and Tryptophan Time-Resolved UV Resonance Raman Signals, *J. Am. Chem. Soc. 111*, 3457−3459.
51. Rodgers, K., Su, S., Subramaniam, S., and Spiro, T. (1992) Hemoglobin R → T Structural Dynamics from Simultaneous Monitoring of Tyrosine and Tryptophan Time-Resolved UV Resonance Raman Signals, *J. Am. Chem. Soc. 114*, 3697−3709.
52. Mukerji, I., and Spiro, T. G. (1994) Modeling the hemoglobin switchpoint with cyanomet valency hybrids: Raman spectroscopic probes of tertiary and quaternary structure, *Biochemistry 33*, 13132−13139.
53. Samuni, U., Navati, M. S., Juszczak, L. J., Dantsker, D., Yang, M., and Friedman, J. M. (2000) Unfolding and refolding of sol−gel encapsulated carbonmonoxymyoglobin: An orchestrated spectroscopic study of intermediates and kinetics? *J. Phys. Chem. B 104*, 10802−10813.

54. Hu, X., and Spiro, T. G. (1997) Tyrosine and tryptophan structure markers in hemoglobin ultraviolet resonance Raman spectra: mode assignments via subunit-specific isotope labeling of recombinant protein, *Biochemistry 36*, 15701−15712.
55. Wang, D., Zhao, X., Shen, T.-J., Ho, C., and Spiro, T. (1999) Role of Interhelical H-Bonds [Wα14-Tα67 and Wβ15-Sβ72] in the Hemoglobin Allosteric Reaction Path Evaluated by UV Resonance Raman Spectroscopy of Site-Mutants, *J. Am. Chem. Soc. 121*, 11197−11203.
56. Nagai, M., Kaminaka, S., Ohba, Y., Nagai, Y., Mizutani, Y., and Kitagawa, T. (1995) Ultraviolet resonance Raman studies of quaternary structure of hemoglobin using a tryptophan β37 mutant, *J. Biol. Chem. 270*, 1636−1642.
57. Huang, S., Peterson, E. S., Ho, C., and Friedman, J. M. (1997) Quaternary structure sensitive tyrosine interactions in hemoglobin: a UV resonance Raman study of the double mutant rHb (β99Asp → Asn, α42Tyr → Asp), *Biochemistry 36*, 6197−6206.
58. Wang, D., Zhao, X., and Spiro, T. G. (2000) Chain Selectivity of Tyrosine Contributions to Hemoglobin Static and Time-Resolved UVRR Spectra in C Isotopic Hybrids, *J. Phys. Chem. 104*, 4149−4152.
59. Wang, D., and Spiro, T. G. (1998) Structure changes in hemoglobin upon deletion of C-terminal residues, monitored by resonance Raman spectroscopy, *Biochemistry 37*, 9940−9951.
60. Kwiatkowski, L. D., Hui, H. L., Wierzba, A., Noble, R. W., Walder, R. Y., Peterson, E. S., Sligar, S. G., and Sanders, K. E. (1998) Preparation and kinetic characterization of a series of βW37 variants of human hemoglobin A: evidence for high-affinity T quaternary structures, *Biochemistry 37*, 4325−4335.
61. Gray, R. D. (1980) The effect of H^+, inositol hexaphosphate, and Zn(II) on the tetramer-dimer equilibrium of liganded hemoglobin, *J. Biol. Chem. 255*, 1812−1818.
62. Gray, R. D., and Gibson, Q. H. (1971) The effect of inositol hexaphosphate on the kinetics of CO and O_2 binding by human hemoglobin, *J. Biol. Chem. 246*, 7168−7174.
63. Gray, R. D., and Dean, W. L. (1987) The effect of 2,3-diphosphoglycerate on the tetramer-dimer equilibrium of carbon monoxide hemoglobin in dilute solution. Correlation between sedimentation and kinetic behavior, *J. Biol. Chem. 262*, 15890−15893.
64. Safo, M. K., Burnett, J. C., Musayev, F. N., Nokuri, S., and Abraham, D. J. (2002) Structure of human carbonmonoxyhemoglobin at 2.16 Å: a snapshot of the allosteric transition, *Acta Crystallogr. D58*, 2031−2037.
65. Chatterjee, R., Walder, R. Y., Arnone, A., and Walder, J. A. (1982) Mechanism for the increase in solubilty of deoxyhemoglobin S due to cross-linking the β chains between lysine-82β1 and lysine-82β2, *Biochemistry 21*, 5901−5909.
66. Ascenzi, P., Bertollini, A., Coletta, M., Desideri, A., Giardina, B., Polizio, F., Santucci, R., Scatena, R., and Amiconi, G. (1993) Cooperative effect of inositol hexakisphosphate, bezafibrate, and clofibric acid on the spectroscopic properties of the nitric oxide derivative of ferrous human hemoglobin, *J. Inorg. Biochem. 50*, 263−272.
67. Coletta, M., Angeletti, M., Ascenzi, P., Bertollini, A., Della Longa, S., De Sanctis, G., Priori, A. M., Santucci, R., and Amiconi, G. (1999) Coupling of the oxygen-linked interaction energy for inositol hexakisphosphate and bezafibrate binding to human HbA0, *J. Biol. Chem. 274*, 6865−6874.
68. Abraham, D. J., Safo, M. K., Boyiri, T., Danso-Danquah, R. E., Kister, J., and Poyart, C. (1995) How allosteric effectors can bind to the same protein residue and produce opposite shifts in the allosteric equilibrium, *Biochemistry 34*, 15006−15020.
69. Safo, M. K., Moure, C. M., Burnett, J. C., Joshi, G. S., and Abraham, D. J. (2001) High-resolution crystal structure of deoxy hemoglobin complexed with a potent allosteric effector, *Protein Sci. 10*, 951−957.
70. Safo, M. K., Boyiri, T., Burnett, J. C., Danso-Danquah, R., Moure, C. M., Joshi, G. S., and Abraham, D. J. (2002) X-ray crystallographic analyses of symmetrical allosteric effectors of hemoglobin: compounds designed to link primary and secondary binding sites, *Acta Crystallogr. D58*, 634−644.
71. Perutz, M. F., Shih, D. T., and Williamson, D. (1994) The chloride effect in human haemoglobin. A new kind of allosteric mechanism, *J. Mol. Biol. 239*, 555−560.
72. Bonaventura, J., Bonaventura, C., Sullivan, B., and Godette, G. (1975) Hemoglobin Deer Lodge (β2 His replaced by Arg). Consequences of altering the 2,3-diphosphoglycerate binding site, *J. Biol. Chem. 250*, 9250−9255.
73. Ascenzi, P., Coletta, M., Desideri, A., Polizio, F., Bertollini, A., Santucci, R., and Amiconi, G. (1992) Effect of bezafibrate and clofibric acid on the spectroscopic properties of the nitric oxide derivative of ferrous human hemoglobin, *J. Inorg. Biochem. 48*, 47−53.
74. Egawa, T., Tsuneshigi, A., and Yonetani, T. (2003) Isothermal titration calorimetry of the binding thermodynamics of heterotropic alloseric effectors to carbonmonoxy hemoglobin, *Biophys. J. 84*, 33a.
75. Shibayama, N., Miura, S., Tame, J. R., Yonetani, T., and Park, S. Y. (2002) Crystal structure of horse carbonmonoxyhemoglobin-bezafibrate complex at 1.55-Å resolution. A novel allosteric binding site in R-state hemoglobin, *J. Biol. Chem. 277*, 38791−38796.
76. Wireko, F. C., Kellogg, G. E., and Abraham, D. J. (1991) Allosteric modifiers of hemoglobin. 2. Crystallographically determined binding sites and hydrophobic binding/interaction analysis of novel hemoglobin oxygen effectors, *J. Med. Chem. 34*, 758−767.
77. Abraham, D. J., Wireko, F. C., Randad, R. S., Poyart, C., Kister, J., Bohn, B., Liard, J. F., and Kunert, M. P. (1992) Allosteric modifiers of hemoglobin: 2-[4-[[(3,5-disubstituted anilino)carbonyl]methyl]phenoxy]-2-methylpropionic acid derivatives that lower the oxygen affinity of hemoglobin in red cell suspensions, in whole blood, and in vivo in rats, *Biochemistry 31*, 9141−9149.
78. Kavanaugh, J. S., Weydert, J. A., Rogers, P. H., and Arnone, A. (1998) High-resolution crystal structures of human hemoglobin with mutations at tryptophan 37β: structural basis for a high-affinity T-state, *Biochemistry 37*, 4358−4373.
79. Wajcman, H., Kister, J., Galacteros, F., Spielvogel, A., Lin, M. J., Vidugiris, G. J., Hirsch, R. E., Friedman, J. M., and Nagel, R. L. (1996) Hb Montefiore (126(H9)Asp → Tyr). High oxygen affinity and loss of cooperativity secondary to C-terminal disruption, *J. Biol. Chem. 271*, 22990−22998.
80. Samuni, U., Juszczak, L., Dantsker, D., Khan, I., Friedman, A. J., Perez-Gonzalez-de-Apodaca, J., Bruno, S., Hui, H. L., Colby, J. E., Karasik, E., Kwiatkowski, L. D., Mozzarelli, A., Noble, R., and Friedman, J. M. (2003) Functional and spectroscopic characterization of half-liganded iron−zinc hybrid hemoglobin: evidence for conformational plasticity within the T state, *Biochemistry 42*, 8272−8288.
81. Dick, L. A., Heibel, G., Moore, E. G., and Spiro, T. G. (1999) UV resonance Raman spectra reveal a structural basis for diminished proton and CO_2 binding to α,α-cross-linked hemoglobin, *Biochemistry 38*, 6406−6410.
82. Dave, B. C., Dunn, B., Valentine, J. S., and Zink, J. I. (1994) Sol−Gel Encapsulation Methods for Biosensors, *Anal. Chem. 66*, 1120A−1127A.
83. Dave, B. C., Miller, J. M., Dunn, B., Valentine, J. S., and Zink, J. I. (1997) Encapsulation of Proteins in Bulk and Thin Film Sol−Gel Matrices, *J. Sol−Gel Sci. Technol. 8*, 629−634.
84. Ellerby, L. M., Nishida, C. R., Nishida, F., Yamanaka, S. A., Dunn, B., Valentine, J. S., and Zink, J. I. (1992) Encapsulation of proteins in transparent porous silicate glasses prepared by the sol−gel method, *Science 255*, 1113−1115.
85. Eggers, D. K., and Valentine, J. S. (2001) Molecular confinement influences protein structure and enhances thermal protein stability, *Protein Sci. 10*, 250−261.
86. Arnone, A., and Williams, D., Jr., INSERM, 18−19 July, 2003, Vol. 70, pp 15−22.

BI035481O